

# Granger Causality in High-Dimensional Networks of Time Series

Sipan Aslan & Hernando Ombao

Statistics Program, KAUST

King Abdullah University of Science and Technology

Thuwal, KSA, 29355-6900

sipan.aslan@kaust.edu.sa

hernando.ombao@kaust.edu.sa

**Abstract**—A novel approach is developed for discovering directed connectivity between specified pairs of nodes in a high-dimensional network (HDN) of brain signals. To accurately identify causal connectivity for such specified objectives, it is necessary to properly address the influence of all other nodes within the network. The proposed procedure herein starts with the estimation of a low-dimensional representation of the other nodes in the network utilizing (frequency-domain-based) spectral dynamic principal component analysis (sDPCA). The resulting scores can then be removed from the nodes of interest, thus eliminating the confounding effect of other nodes within the HDN. Accordingly, causal interactions can be dissected between nodes that are isolated from the effects of the network. Extensive simulations have demonstrated the effectiveness of this approach as a tool for causality analysis in complex time series networks. The proposed methodology has also been shown to be applicable to multichannel EEG networks.

**Index Terms**—High-Dimensional Networks of Signals, Connectivity, Causality, Spectral Dynamic PCA, EEG signals

## I. INTRODUCTION

Identifying effective connectivity in high-dimensional networks (HDN) is a challenging problem that remains an active area of research and has been previously addressed by several studies [see, e.g., 1, 2, 3, 4, 5, 6, 7, 8]. Moreover, it is difficult to infer or interpret interactions between a pair of nodes while taking into account potential interactions with all other nodes in the background [9, 10]. This is a particularly relevant issue (e.g., analysis of EEG-like signals) when the focus might stand on a few channels/nodes of interest (COI/NOI) within an extensive network of interacting nodes. In fact, utilizing conventional vector autoregressive models (VAR) can be a practical way to identify pairwise causal interactions in high-dimensional networks as long as the potential confounding effect due to the high-dimensional background nodes is addressed. In this paper, we propose a framework that provides a low-dimensional summary of the background activity in the high-dimensional network (HDN).

To discern effective connectivity, particularly between pairs of nodes in an HDN of brain signals, we propose a practical and easily accessible approach based on spectral dynamic principal component analysis (PCA) ([11, 12]) combined with testing for GC in lieu of the conventional F-test.

The sDPCA method enhances the classical PCA by incorporating temporal dependency within the data, thereby reducing

the dimensionality of time series in the frequency domain while retaining maximal temporal information. In other words, while the classical PCA is based on the eigendecomposition of the zero-lag (or contemporaneous) covariance matrix, sDPCA is based on the eigendecomposition of the spectral matrix at all frequencies. Since there is a 1-1 relationship between the spectral matrix (at all frequencies) and the covariance matrix (at all lags) then this approach captures lead-lag relationships amongst signals.

Various methodologies have evolved from sDPCA. For instance, [13] developed a spectral envelope using sDPCA to identify common signals across multiple time series, while [14] proposed a functional variant of sDPCA for analyzing functional time-series data. As indicated by [15, 5, 16], spectral principal component analysis (sPCA) in the frequency domain offers practical benefits and is highly effective in low-dimensional representations of high-dimensional time series. The main objective of this study is to illustrate how the proposed approach enables the practical and sufficient isolation of COI by partialling out the influence of disinterested nodes, which are derived as a dynamic summary in a low-dimensional representation. The frequency-domain dynamic PCA method maintains the spectral characteristics of the data, which are crucial for accurately determining causal relationships in time series networks.

The proposed approach offers two main advantages. Firstly, sDPCA in the frequency domain offers an accurate and practical dimension reduction while preserving the spectral information. This is essential because the spectrum of a signal captures cross-covariances at all lags. This leads to a more precise isolation of COI, reducing the likelihood of spurious causal inferences. Secondly, the proposed approach enables the formation of a comprehensive yet interpretable representation of the interactions between specified nodes at a defined level of resolution rather than being unable to infer by the expansive number of possible interactions between nodes. This facilitates the study of considerable numbers of interactions, ranging from pairs of nodes to interactions between a tractable number of clusters of nodes. The subsequent sections will elaborate on the proposed approach and its components. Section 2 presents the proposed approach. Section 3 outlines the scope of the simulation study and presents related results. Section 4 applies the proposed approach to EEG data and discusses the findings.

## II. METHODOLOGY

### A. Inference in high-dimensional networks of time series

Define  $N = \{Y_t^*, X_t^*, Z_{1,t}, \dots, Z_{n-2,t}\}$  to be a high dimensional network of signals with possibly  $n \geq 256$  nodes. As we consider in this paper, this network may represent the activity of a brain through EEG recordings in which each component (i.e., node or channel) is actually a time series. In this notation of network  $N$ ,  $Y^*$  and  $X^*$  denote any two nodes of interest. For problems whose solutions are sought component-wise, we set our goal as exploring the interaction or efficient connectivity between any pair of nodes in a network rather than the relationality of the whole network. These two nodes are subject to the influence of other nodes due to the network's relational structure. This means that to dissect the respective efficient connection between any two nodes of interest; they need to be freed from the influences of other nodes. Thereby, the interference-free counterparts of the nodes of interest can be obtained in the following manner:

$$Y_t = Y_t^* - E(Y_t^* | f_z(Z_{1,t}, \dots, Z_{n-2,t})),$$

$$X_t = X_t^* - E(X_t^* | f_z(Z_{1,t}, \dots, Z_{n-2,t})),$$

where the  $f_z(\cdot)$  is a function that encompasses the dynamic variability of excluded nodes. Practically, the function  $f_z(\cdot)$  acts as a filter and can take any form as long as it provides the net summary discharge of the nodes excluded. Within the scope of this study, we utilize the spectral domain dynamic PCA implementation made available by Hörmann et al. (2015) via R package called `freqdom`. This method, originally proposed by Brillinger (1981), enables us to obtain principal component scores that concisely encapsulate variability in multi-dimensional time series, specifically with regard to their serial dependence [17, 16, see, e.g., ]. Hence, we propose the filter  $f_z(\cdot)$  over excluded nodes to provide the following summary indicators,

$$f_z(Z_{1,t}, \dots, Z_{n-2,t}) = \{pc1, pc2, \dots, pc_k, \text{interactions}\},$$

where  $pc1, pc2, \dots, pc_k$  are the scores of the principal components obtained through sDPCA, and interactions represent any interaction terms between these principal components.

The conditional means with respect to these indicators are then given by:

$$E(Y_t^* | f_z(Z_{1,t}, \dots, Z_{n-2,t})) = a_1 \cdot pc1 + a_2 \cdot pc2 + \dots + a_k \cdot pc_k + \sum a_{ij} \cdot (pc_i \times pc_j),$$

$$E(X_t^* | f_z(Z_{1,t}, \dots, Z_{n-2,t})) = b_1 \cdot pc1 + b_2 \cdot pc2 + \dots + b_k \cdot pc_k + \sum b_{ij} \cdot (pc_i \times pc_j),$$

where  $pc_i$  represents the score of the  $i$ -th dynamic principal component and  $a_i, b_i, a_{ij}, b_{ij}$  are coefficients corresponding to the principal components and their interactions. The number

of principal components  $k$  can be chosen to be relatively low compared to the number of dimensions, provided that they capture a sufficient proportion of the total variability in the network. For practical implementation, the first few principal components are generally sufficient.

a) *Spectral DPCA*: The frequency domain dynamic PCA decomposes a multivariate time series into uncorrelated components in the frequency domain, maximizing the long-run variance explained. Unlike classical PCA, which produces components uncorrelated in space, sDPCA focuses on the spectral density of the data, producing components uncorrelated in time.

Assume a multivariate time series  $\mathbf{Z}$  of dimension  $T \times n$ , where  $T$  is the number of time points, and  $n$  is the number of variables; this can be considered as a network of time series. The first step in sDPCA involves estimating the spectral density matrix  $F(\omega)$  from the time series. The cross-spectral density for  $\mathbf{Z}$  can be defined as:

$$F_{\mathbf{Z}}(\omega) = \sum_{h \in \mathbb{Z}} \text{Cov}(\mathbf{Z}_h, \mathbf{Z}_0) \exp(-2\pi i h \omega),$$

where  $\text{Cov}(\mathbf{Z}_h, \mathbf{Z}_0)$  is the auto-covariance matrix at lag  $h$ . The empirical cross-spectral density can be estimated using a windowed version of the lagged auto-covariance matrices:

$$\hat{F}_{\mathbf{Z}}(\omega) = \sum_{|h| \leq q} w\left(\frac{|h|}{q}\right) \hat{C}_{\mathbf{Z}}(h) \exp(-2\pi i h \omega),$$

where  $w(\cdot)$  is a window function (i.e., kernel),  $q$  is the window size, and  $\hat{C}_{\mathbf{Z}}(h)$  is the empirical lagged auto-covariance given by:

$$\hat{C}_{\mathbf{Z}}(h) = \frac{1}{T} \sum_{t=1}^{T-|h|} (\mathbf{Z}_{t+|h|} - \bar{\mathbf{Z}})(\mathbf{Z}_t - \bar{\mathbf{Z}})',$$

for  $h \geq 0$ , and

$$\hat{C}_{\mathbf{Z}}(h) = \hat{C}_{\mathbf{Z}}(-h)' = \frac{1}{T} \sum_{t=1}^{T+h} (\mathbf{Z}_t - \bar{\mathbf{Z}})(\mathbf{Z}_{t-h} - \bar{\mathbf{Z}})'$$

for  $h < 0$ .

Once the spectral density matrix  $F(\omega)$  is obtained, the dynamic principal component filters  $\phi_k^{(j)}$  are computed, where  $k \in [-q, q] \subset \mathbb{Z}$  and the index  $j$  is referring to the  $j$ -th largest dynamic eigenvalue. The filters are derived as the Fourier coefficients of the dynamic eigenvectors  $\varphi_j(\omega)$  of the spectral density matrix  $F(\omega)$ :

$$\phi_k^{(j)} = \frac{1}{2\pi} \int_{-\pi}^{\pi} \varphi_j(\omega) e^{-ik\omega} d\omega.$$

The dynamic principal component scores  $dpc_t^{(j)}$  are then calculated by filtering the time series  $\mathbf{Z}_t$  with the dynamic principal component filters:

$$dpc_t^{(j)} = \sum_{k=-q}^q \phi_k^{(j)} \mathbf{Z}_{t-k}.$$

This convolution operation can be represented in matrix notation as:

$$\mathbf{dpc} = \mathbf{Z} * \Phi,$$

where  $*$  denotes the convolution operation.

The proportion of variance explained by the  $j$ -th dynamic principal component is quantified as:

$$v_j = \frac{\int_{-\pi}^{\pi} \lambda_j(\omega) d\omega}{\int_{-\pi}^{\pi} \text{tr}(F(\omega)) d\omega},$$

where  $\lambda_j(\omega)$  is the  $j$ -th dynamic eigenvalue of the spectral density matrix  $F(\omega)$ . This ratio provides a measure of how much of the total variance in the time series is captured by each dynamic principal component.

In summary, the sDPCA method involves estimating the spectral density matrix from the time series data using windowed empirical lagged auto-covariances and Fourier transform, computing dynamic principal component filters by performing eigendecomposition on the spectral density matrix and applying the inverse Fourier transform to the dynamic eigenvectors, obtaining dynamic principal component scores by filtering the time series with the computed filters, and quantifying the proportion of variance explained by each dynamic principal component. These steps collectively facilitate the decomposition of multivariate time series into components that are uncorrelated in time and maximize the long-run variance explained.

#### b) Terms and Notation:

- $\mathbf{Z}$ : Original multivariate time series matrix of dimensions  $T \times n$ , where  $T$  is the number of time points and  $n$  is the number of variables.
- $F_{\mathbf{Z}}(\omega)$ : Cross-spectral density matrix at frequency  $\omega$ .
- $\text{Cov}(\mathbf{Z}_h, \mathbf{Z}_0)$ : Covariance matrix at lag  $h$ .
- $\hat{\mathbf{C}}_{\mathbf{Z}}(h)$ : Empirical lagged auto-covariance matrix at lag  $h$ .
- $w(\cdot)$ : Window function used to smooth the estimates.
- $q$ : Window size for the kernel estimator.
- $\phi_k^{(j)}$ : Dynamic principal component filters, obtained as the Fourier coefficients of the dynamic eigenvectors.
- $\varphi_j(\omega)$ : Dynamic eigenvectors of the spectral density matrix  $F(\omega)$ .
- $dpc_t^{(j)}$ : Dynamic principal component scores.
- $\mathbf{dpc}$ : Matrix of dynamic principal component scores.
- $\Phi$ : Matrix of dynamic principal component filters.
- $\lambda_j(\omega)$ :  $j$ -th dynamic eigenvalue of the spectral density matrix  $F(\omega)$ .

### B. Granger Causality test

Granger Causality (GC) is a statistical hypothesis test used to determine whether one time series can predict another. The concept, introduced by Granger (1969), is based on the principle that if the prediction of a time series  $Y_t$  can be improved by incorporating past values of another time series  $X_t$ , then  $X_t$  is said to "Granger-cause"  $Y_t$ .

The Granger causality test involves the following steps. First, consider two time series  $X_t$  and  $Y_t$ . To test if  $X_t$  Granger-causes  $Y_t$ , we compare the following two models:

- Unrestricted Model:

$$Y_t = \alpha_0 + \sum_{i=1}^p \alpha_i Y_{t-i} + \sum_{j=1}^q \beta_j X_{t-j} + \epsilon_t$$

- Restricted Model:

$$Y_t = \gamma_0 + \sum_{i=1}^p \gamma_i Y_{t-i} + \eta_t$$

Here,  $p$  and  $q$  are the maximum lags considered,  $\alpha_0$  and  $\gamma_0$  are constants,  $\alpha_i$  and  $\gamma_i$  are coefficients of the lagged  $Y_t$ ,  $\beta_j$  are coefficients of the lagged  $X_t$ , and  $\epsilon_t$  and  $\eta_t$  are error terms.

To determine if  $X_t$  Granger-causes  $Y_t$ , we test the null hypothesis:

$$H_0 : \beta_1 = \beta_2 = \dots = \beta_q = 0$$

against the alternative hypothesis:

$$H_1 : \text{At least one } \beta_j \neq 0 \text{ for } j = 1, 2, \dots, q$$

The test statistic is based on the F-distribution and is computed as:

$$F = \frac{(RSS_R - RSS_U)/q}{RSS_U/(T - p - q - 1)},$$

where  $RSS_R$  and  $RSS_U$  are the residual sum of squares of the restricted and unrestricted models, respectively, and  $T$  is the number of observations. If the computed F-statistic is greater than the critical value from the F-distribution, we reject the null hypothesis, concluding that  $X_t$  Granger-causes  $Y_t$ .

Granger causality is widely used in fields such as economics, neuroscience, and environmental sciences. In neuroscience, it helps to understand the directional interactions between brain regions by analyzing EEG or fMRI data. However, conventional GC assumes that error terms are normally distributed and homoscedastic, which is often violated in practice, especially in EEG time series that exhibit heteroscedasticity and fat-tailed distributions. These violations can bias results.

Unobserved confounders can also complicate GC analysis. If external variables influencing both time series are omitted, the test might falsely identify causal relationships. This issue is particularly acute in complex systems with many interacting variables.

### C. Proposed Approach

In high-dimensional networks of time series, analyzing causal connectivity between specific pairs of signals can be both challenging and computationally intensive due to the complexity of modeling interactions across all nodes. The approach to be followed would be to model the whole material if there were no high dimensionality problems. However, modeling under high dimensionality requires fitting highly parameterized models to the entire network, leading to difficult-to-interpret estimates and an increased risk of overfitting. To overcome these challenges, we propose a practical and easily implementable method that focuses on isolating the nodes/channels of interest by effectively reducing the dimensionality of the network. Our approach utilizes spectral dynamic principal component analysis to capture the essential variability of the background network in a

low-dimensional representation. By partialling out the influence of other nodes through sDPCA, we can isolate the COI and accurately assess the causal connectivity between them using conventional Granger causality tests. This method simplifies the analysis by avoiding the need to model the entire high-dimensional network and enhances interpretability when the primary interest is in the causal relationship between specific signals. The proposed approach is given in the **Procedure** outline below.

### III. SIMULATION STUDY

The aim of this simulation study is to evaluate the effectiveness of spectral dynamic principal component analysis (sDPCA) combined with Granger causality (GC) testing in identifying true causal relationships within a high-dimensional network of time series data, specifically focusing on EEG-like data. The study investigates how well the proposed method isolates the channels of interest (COI) from the influences of other channels and accurately assesses their causal interactions. We conduct two sets of simulations: one with linear influences and another with nonlinear influences.

#### A. Linear Scheme

In the linear scheme of the simulation study, we generate a network of time series data with predefined causal relationships and linear influences from additional channels.

1) *Generating Initial Channels:* We begin by generating  $N = 40$  initial time series channels, denoted by  $\{Z_i(t)\}_{i=1}^N$ , over time points  $t = 1, \dots, T$ . The channels are divided into  $N/2 = 20$  causal pairs, where each pair consists of a "cause" and an "effect" channel.

For each cause channel  $Z_i(t)$ , where  $i = 1, \dots, N/2$ , we model it as a weighted sum of latent processes representing different EEG frequency bands plus noise:

$$Z_i(t) = a_i \delta(t) + b_i \theta(t) + c_i \alpha(t) + d_i \beta(t) + e_i \gamma(t) + \varepsilon_i(t),$$

where:

- $\delta(t)$ ,  $\theta(t)$ ,  $\alpha(t)$ ,  $\beta(t)$ , and  $\gamma(t)$  are latent processes corresponding to the EEG frequency bands:
  - Delta (0.5–4 Hz):  $\delta(t)$ ,
  - Theta (4–8 Hz):  $\theta(t)$ ,
  - Alpha (8–12 Hz):  $\alpha(t)$ ,
  - Beta (12–30 Hz):  $\beta(t)$ ,
  - Gamma (> 30 Hz):  $\gamma(t)$ .

Each latent process is modeled as an autoregressive process of order 2 (AR(2)):

$$\nu(t) = \phi_{1\nu} \nu(t-1) + \phi_{2\nu} \nu(t-2) + \eta_\nu(t), \quad \nu \in \{\delta, \theta, \alpha, \beta, \gamma\},$$

where  $\eta_\nu(t)$  is white noise. The AR coefficients can be expressed in terms of  $r_\nu$  and  $\varrho_\nu$ :

$$\phi_{1\nu} = 2r_\nu \cos(\varrho_\nu),$$

$$\phi_{2\nu} = -r_\nu^2.$$

where  $r_\nu$  is the damping factor, chosen close to 1 (e.g.,  $0.8 \leq r_\nu < 1$ ) to ensure stationarity and control the

---

### Procedure: Identifying Causal Connectivity in HDN

---

**Input:** High-dimensional Networks of Signals

$$N = \{Y_t^*, X_t^*, Z_{1,t}, \dots, Z_{n-2,t}\}$$

**Output:** Determination of causal relationship between  $Y_t^*$  and  $X_t^*$

**1. Identify Nodes of Interest:** NOI:  $\{Y_t^*, X_t^*\}$ .

In practice, each node can also be a cluster of nodes that can be represented by sDPCA scores.

**2. Apply sDPCA:**

i Estimate spectral density matrix  $F_{\mathbf{Z}}(\omega)$  for  $\mathbf{Z}_t = \{Z_{1,t}, \dots, Z_{n-2,t}\}$ .

ii Compute dynamic eigenvectors  $\varphi_j(\omega)$  and eigenvalues  $\lambda_j(\omega)$ .

iii Derive dynamic principal component filters:

$$\phi_k^{(j)} = \frac{1}{2\pi} \int_{-\pi}^{\pi} \varphi_j(\omega) e^{-ik\omega} d\omega$$

iv Calculate dynamic principal component scores:

$$\text{dpc}_t^{(j)} = \sum_{k=-q}^q \phi_k^{(j)} \mathbf{Z}_{t-k}$$

**3. Partial Out Influence of Other Nodes:**

$$Y_t = Y_t^* - \hat{E}(Y_t^* | \text{dpc}_t^{(1)}, \dots, \text{dpc}_t^{(k)})$$

$$X_t = X_t^* - \hat{E}(X_t^* | \text{dpc}_t^{(1)}, \dots, \text{dpc}_t^{(k)})$$

**4. Fit Restricted/Unrestricted Models:**

Unrestricted Model:

$$Y_t = \alpha_0 + \sum_{i=1}^p \alpha_i Y_{t-i} + \sum_{j=1}^q \beta_j X_{t-j} + \epsilon_t$$

Restricted Model:

$$Y_t = \gamma_0 + \sum_{i=1}^p \gamma_i Y_{t-i} + \eta_t$$

**5. Perform Granger Causality Tests:**

i Test null hypothesis  $H_0 : \beta_j = 0$  for all  $j$  in the equation for  $Y_t$ .

ii Compute F-statistic:

$$F = \frac{(RSS_R - RSS_U)/q}{RSS_U/(T - K)}$$

where:

- $RSS_R$ : Residual sum of squares of restricted model (without  $X_{t-j}$  terms).
- $RSS_U$ : Residual sum of squares of unrestricted model.
- $q$ : Number of restrictions (parameters set to zero).
- $K$ : Total number of parameters in the unrestricted model.

iii Compare F-statistic with critical value from  $F$ -distribution  $F_{q, T-K}$ .

iv Reject  $H_0$  if  $F$  exceeds critical value; conclude  $X_t$  Granger-causes  $Y_t$ .

v Repeat steps for testing causality from  $Y_t$  to  $X_t$ .

---

bandwidth of the spectral peak. And,  $\varrho_\nu$  is the angular frequency (in radians per sample), related to the desired

frequency  $f_\nu$  (in Hz) by:

$$Q_\nu = 2\pi \frac{f_\nu}{f_s},$$

with  $f_s$  being the sampling frequency. By modeling the latent processes to correspond to specific EEG frequency bands, we aim to simulate EEG-like signals more realistically.

- $a_i, b_i, c_i, d_i,$  and  $e_i$  are random weights drawn from a uniform distribution to ensure variability among channels.
- $\varepsilon_i(t)$  is white noise added to each channel.

For each effect channel  $Z_j(t)$ , where  $j = i + N/2$  and  $i = 1, \dots, N/2$ , we generate it as an autoregressive process influenced by its corresponding cause channel:

$$Z_j(t) = \sum_{k=1}^p \phi_k Z_i(t-k) + \varepsilon_j(t),$$

where:

- $p = 2$  is the order of the autoregressive process.
- $\phi_k$  are AR coefficients ensuring the stability of the process.
- $\varepsilon_j(t)$  is white noise added to the effect channel.

2) *Extending the Network:* We extend the network by generating additional  $N_{\text{ext}} = 472$  channels, resulting in a total of  $N_{\text{expanded}} = 512$  channels. These additional channels  $\{Z_i(t)\}_{i=N+1}^{N_{\text{expanded}}}$  are generated similarly to the cause channels but without being part of the predefined causal pairs:

$$Z_i(t) = a_i \delta(t) + b_i \theta(t) + c_i \alpha(t) + d_i \beta(t) + e_i \gamma(t) + \varepsilon_i(t).$$

3) *Introducing Linear Influences:* To simulate the effect of a high-dimensional network on the initial channels, we introduce linear influences from a subset of the additional channels. We select a set of connected nodes  $\mathcal{C} \subset \{N+1, \dots, N_{\text{expanded}}\}$  of size  $\text{nofcn}$  (number of connected nodes).

For each initial channel  $Z_i(t)$ ,  $i = 1, \dots, N$ , we randomly select  $k$  influencing nodes from  $\mathcal{C}$  and assign influence weights  $W_{ij}$  drawn from a uniform distribution.

The linear influence on channel  $i$  at time  $t$  is defined as:

$$L_i(t) = \sum_{j \in \mathcal{I}_i} W_{ij} Z_j(t),$$

where  $\mathcal{I}_i$  is the set of influencing nodes for channel  $i$ . For each initial channel  $Z_i(t)$  and each influencing node  $Z_j(t) \in \mathcal{I}_i$ , we assign an influence weight  $W_{ij}$  drawn from a uniform distribution centered around a specified influence weight  $\omega$ :

$$W_{ij} \sim \text{Uniform}\left(\omega - \frac{\omega}{16}, \omega + \frac{\omega}{16}\right), \quad \text{for } j \in \mathcal{I}_i.$$

We then update the initial channels by adding the linear influence:

$$\tilde{Z}_i(t) = Z_i(t) + L_i(t).$$

The updated initial channels  $\tilde{Z}_i(t)$  now contain both their original dynamics and the linear influence from the connected nodes.

## B. Nonlinear Scheme

In the nonlinear scheme, we introduce moderate nonlinearity into the influence of the connected nodes on the initial channels to study the robustness of the sDPCA and GC testing framework under nonlinear conditions.

1) *Introducing Nonlinear Influences:* Similar to the linear simulation, we select a set of connected nodes  $\mathcal{C}$  and assign influence weights  $W_{ij}$  for each initial channel  $Z_i(t)$ .

The linear influence is computed as before:

$$L_i(t) = \sum_{j \in \mathcal{I}_i} W_{ij} Z_j(t).$$

To introduce nonlinearity, we compute interaction terms between the influencing nodes for each initial channel:

$$Q_i(t) = \sum_{j \in \mathcal{I}_i} \sum_{k > j} W_{ij} W_{ik} Z_j(t) Z_k(t).$$

We apply a nonlinear function  $f(\cdot)$  to the linear influence, such as the softplus function:

$$f(x) = \ln(1 + e^x).$$

The total influence on channel  $i$  at time  $t$  is then given by:

$$S_i(t) = f(L_i(t)) + \omega Q_i(t),$$

where  $\omega$  is a scaling parameter controlling the magnitude of the nonlinear interaction influence.

We update the initial channels with the total influence:

$$\tilde{\tilde{Z}}_i(t) = Z_i(t) + S_i(t).$$

## C. Removing Influences

1) *Removing Influences Using sDPCA:* To isolate the channels of interest from the influences of the connected nodes, we apply sDPCA to the time series data of the connected nodes  $\{Z_j(t)\}_{j \in \mathcal{C}}$ . We obtain principal component scores  $\{Z_{\text{pc},k}(t)\}_{k=1}^{N_{\text{dpc}}}$ , where  $N_{\text{dpc}}$  is the number of dynamic principal components retained. For each adjusted initial channel  $\tilde{Z}_i(t)$ , we regress it on the principal component scores and their interaction terms:

$$\tilde{\tilde{Z}}_i(t) = \sum_{k=1}^{N_{\text{dpc}}} \varphi_{ik} Z_{\text{pc},k}(t) + \sum_{k \neq l} \psi_{ikl} Z_{\text{pc},k}(t) Z_{\text{pc},l}(t) + \epsilon_i(t).$$

We then use the residuals  $\hat{\epsilon}_i(t)$  as the adjusted time series for further analysis:

$$\hat{Z}_i(t) = \hat{\epsilon}_i(t).$$

2) *Granger Causality Testing:* Using the adjusted time series  $\{\hat{Z}_i(t)\}_{i=1}^N$ , we fit vector autoregressive (VAR) models and perform Granger causality tests to identify causal relationships among the initial channels. The effectiveness of the sDPCA adjustment is evaluated by comparing the detected causal relationships with the ground truth.

#### D. Simulation Results

To evaluate the performance of the proposed method, we compute accuracy metrics based on the detection of true causal relationships. Specifically, we compare the identified causal links with the known ground truth and compute measures such as accuracy rate.

By conducting both linear and nonlinear simulations, we assess the robustness of the sDPCA combined with Granger causality testing in high-dimensional settings with complex interdependencies. The results provide insights into the method’s effectiveness in isolating the channels of interest and accurately detecting causal relationships, even in the presence of nonlinear influences.

The results are sensitive to the choice of latent processes and the influence of other channels. Different scenarios are explored by varying the number of influencing channels and the weight of their influence, with the goal of assessing the robustness and reliability of the proposed method in detecting true causal relationships within high-dimensional time series networks. For example, Table I presents the accuracy results for one of the simulation studies for different numbers of influencing nodes and varying weights on the COI in a high-dimensional network. The COI consists of the first 40 nodes out of a total of 512 nodes. The results of the other 5 simulation studies are given in the appendix.

TABLE I  
ACCURACY RESULTS FOR VARYING NUMBERS OF INFLUENCING NODES WITH NONLINEAR INFLUENCE AND WEIGHTS ON THE COI IN A HIGH-DIMENSIONAL NETWORK UNDER A NON-NORMAL ERROR DISTRIBUTION,  $\epsilon \sim \text{non-Norm}(\mu = -1, \sigma = 1, \gamma = 1.5, \kappa = 3.5)$ . THE COI CONSISTS OF THE FIRST 40 NODES OUT OF A TOTAL OF 512 NODES. THE NUMBERS 30, 60, 90, AND 120 REPRESENT THE NUMBER OF NODES INFLUENCING THE COI, AND THE VALUES 0.1, 0.3, 0.5, AND 0.7 REPRESENT THE WEIGHTS OF THIS INFLUENCE.

Influencing Nodes = 30				
Ndpc	wt. = 0.1	wt. = 0.3	wt. = 0.5	wt. = 0.7
3	0.96	0.88	0.61	0.65
6	0.97	0.77	0.62	0.64
12	0.97	0.82	0.61	0.65
24	0.93	0.82	0.65	0.64
Influencing Nodes = 60				
Ndpc	wt. = 0.1	wt. = 0.3	wt. = 0.5	wt. = 0.7
3	0.98	0.66	0.64	0.64
6	0.99	0.73	0.64	0.65
12	0.94	0.69	0.64	0.64
24	0.96	0.67	0.64	0.64
Influencing Nodes = 90				
Ndpc	wt. = 0.1	wt. = 0.3	wt. = 0.5	wt. = 0.7
3	0.96	0.63	0.63	0.65
6	0.94	0.62	0.64	0.64
12	0.95	0.62	0.64	0.64
24	0.91	0.64	0.64	0.64
Influencing Nodes = 120				
Ndpc	wt. = 0.1	wt. = 0.3	wt. = 0.5	wt. = 0.7
3	0.95	0.65	0.63	0.64
6	0.95	0.65	0.64	0.65
12	0.90	0.64	0.65	0.64
24	0.97	0.64	0.64	0.64

This simulation evaluates the performance of the sDPCA method under a nonlinear influence scheme with non-normal error terms, introducing complexity due to both nonlinearity and deviations from normality.

At a low influence weight (weight = 0.1), sDPCA maintains high accuracy across all numbers of influencing nodes, even as the network becomes super connected and super dense. Accuracy exceeds 0.90 when the number of influencing nodes increases from 30 up to 120, indicating strong robustness in isolating the channels of interest (COI) even in highly interconnected networks where each node affects the causal pairs.

As the influence weight increases to 0.3, accuracy decreases but remains relatively high with fewer influencing nodes. For example, with 30 influencing nodes and  $N_{dpc} = 3$ , the accuracy is 0.88. However, as the network becomes denser (influencing nodes  $\geq 30$ ), the decline in accuracy becomes more pronounced, reflecting the increased challenge of isolating true causal relationships in a super connected network.

At higher influence weights (weight = 0.5 and 0.7), accuracy declines further and stabilizes around 0.64–0.65, regardless of the number of influencing nodes or the number of dynamic principal components ( $N_{dpc}$ ). This plateau suggests a limit to the method’s ability to isolate the COI under strong nonlinear influences and pervasive connectivity, as heavier weights and a denser network make it more challenging to distinguish true causal relationships from spurious ones introduced by nonlinearity and widespread influence.

The impact of increasing  $N_{dpc}$  on accuracy is minimal at higher weights and in denser networks, indicating that adding more principal components does not enhance performance under these conditions. This suggests that the sDPCA method’s capacity to capture and remove complex influences is limited when the network is both highly connected and subject to strong nonlinear interactions.

Overall, the sDPCA method demonstrates robustness to nonlinear influences and non-normal error distributions at lower influence weights and in less densely connected networks. Its effectiveness diminishes as the strength of the nonlinear influence increases and as the network becomes super connected, highlighting the importance of considering both the magnitude of external influences and network connectivity when applying sDPCA in practical settings with nonlinear dynamics.

#### IV. APPLICATION TO EEG DATA

In this section, we apply our proposed approach to real EEG data from an experiment involving motor execution and imagery tasks, offering insights into the temporal dynamics of brain activity. EEG recordings were collected from 109 volunteers using the BCI2000 system with a 64-channel setup; the data is publicly available at PhysioNet.org [18]. Each subject completed 12 task-oriented runs. Participants either physically performed or imagined movements in response to visual cues on a screen, such as opening and closing fists or feet depending on the target’s position. The tasks were divided into four categories: physical movements of the left or right fist, imaginary movements of the left or right fist, physical

movements of both fists or both feet, and imaginary movements of both fists or both feet. EEG data were sampled at 160 Hz, along with an annotation channel indicating rest or the onset of motion (real or imagined) for specific movements. The EEG montage followed the international 10-10 system, omitting certain electrodes (Nz, F9, F10, FT9, FT10, A1, A2, TP9, TP10, P9, and P10).

All data underwent pre-processing to filter out artifacts like eye blinks and muscle movements, preserving the temporal structure of the recordings. The procedure included a high-pass filter at 0.5 Hz to eliminate low-frequency noise, removal of 60 Hz AC line noise, and Independent Component Analysis (ICA) using MNE-Python routines [19, 20] to isolate and exclude artifact components. Finally, artifacts associated with eye blinking and muscle movements were identified and removed, ensuring the recordings were free from these specific interferences.

Despite standard pre-processing, some recordings had unresolved issues like sawtooth traces, excessive blinking, broken channels, and unbalanced epochs. Therefore, we limited our analysis to 35 right-handed subjects (17 females and 18 males) whose recordings were qualified. To demonstrate how the proposed method can dissect causal connections between pairwise nodes in any time series network, we focused on six channels of interest (COI): AF3 and AF4 positioned over the pre-frontal cortex, C3 and C4 placed over the motor cortex, and O1 and O2 over the occipital cortex, as illustrated in Figure 1. These channels were chosen because they correspond to brain regions likely to be active during voluntary movement, imagery, and visual perception.

On the other hand, another important objective is to monitor the effect of the dimension reduction utilizing the sDPCA and its impact on the isolated channels. In particular, we propose that basic statistical tools such as trace plots, serial and partial autocorrelation functions, spectrum estimates, and many more can be practically used to determine the extent to which the method alters time-dependent properties in time series. This helps us to assess the efficacy of the proposed methodology for isolating COI while maintaining the temporal characteristics of the signals.

In Figure 1, we illustrate an example of one epoch from the dataset. The obtained three principal component (PC) scores are plotted over the time series data from which they were derived. This illustrates that the PC scores can capture the temporal structures/dynamics of the high-dimensional time series from which they originate and preserve the main characteristics of the time series.

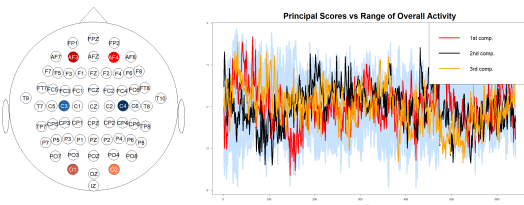


Fig. 1. Isolating Nodes via Spectral Dynamic PCA method

We compared the time-dependent statistical properties before

and after applying the spectral dynamic principal component analysis (PCA) method to the channels of interest. As illustrated in Figures 2, 3 and 4, although the temporal characteristics of the series maintained, there is a noticeable trend toward stationarity in the serial correlation amplitudes, which showed signs of non-stationarity before. This adjustment indicates that while the sequential properties of the series are preserved, they become more aligned with the assumptions required by the auxiliary model used for Granger causality (GC) testing.

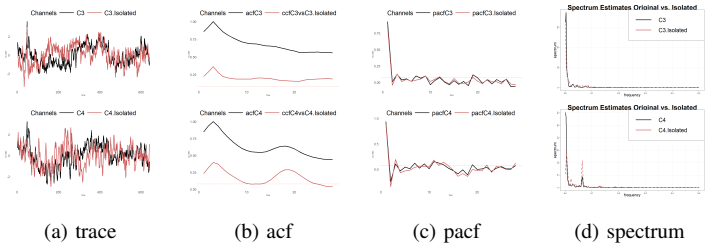


Fig. 2. Sample vs Isolated channels C3 and C4.

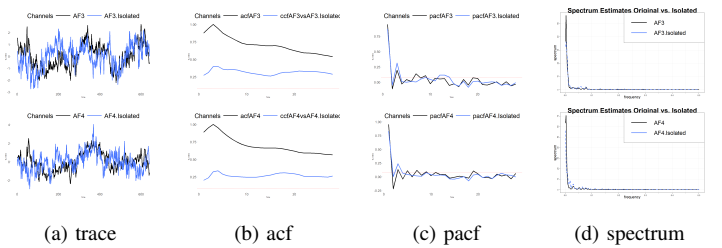


Fig. 3. Sample vs Isolated channels AF3 and AF4.

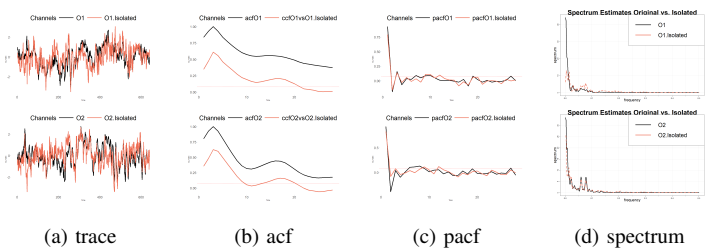


Fig. 4. Sample vs Isolated channels O1 and O2.

Test results given in Table II, reveal significant differences in GC tests conducted before and after the isolation process. In several instances, the GC tests showed contrasting results after the isolation (i.e., dimension reduction), underlining the presence of spurious GC regarding 64-dimensional VAR-based GC analysis. We observed that some of the causal relationships detected in the pre-isolation (i.e., 64-dimensional VAR) were not present in the post-isolation (i.e., 6-dimensional VAR). This suggests that the influences of other channels, when not addressed properly, can lead to misleading conclusions about causality. On the other hand, estimating causal relationships in networks with many time series —using VAR models and Granger Causality tests- is quite challenging, both statistically and computationally. The main issue is the “curse of dimensionality.” As the number of variables increases, the number

TABLE II  
COMPARISON OF GC BEFORE AND AFTER APPLYING SDPCA

Direction of GC	GC test w.r.t 64-dim VAR (Before)	GC test w.r.t 6-dim VAR (After)
C3 → C4	■	■
C3 → AF3	■	□
C3 → AF4	□	■
C3 → O1	■	■
C3 → O2	■	□
C4 → C3	□	■
C4 → AF3	□	□
C4 → AF4	□	■
C4 → O1	□	□
C4 → O2	□	■
AF3 → AF4	□	■
AF3 → C3	□	□
AF3 → C4	□	□
AF3 → O1	□	□
AF3 → O2	□	■
AF4 → AF3	□	■
AF4 → C3	□	□
AF4 → C4	■	■
AF4 → O1	□	□
AF4 → O2	□	□
O1 → O2	□	■
O1 → AF3	■	□
O1 → AF4	□	□
O1 → C3	■	■
O1 → C4	■	□
O2 → O1	□	■
O2 → AF3	□	■
O2 → AF4	□	■
O2 → C3	□	■
O2 → C4	□	□

\*\*Black squares, ■, indicate a "Cause", while white squares, □, represent a "Do not Cause" relationship.

of parameters we need to estimate grows rapidly, leading to a paralyzing parameter space. This can result in overfitting, higher variance in estimators, and problems like multicollinearity when variables are highly correlated. Conventional estimation methods like Ordinary Least Squares (OLS) become unfeasible in this context. Additionally, selecting the right lag order and variables is more complicated with so many variables, increasing the risk of misspecification and inflated type I errors due to multiple testing. On the computational side, high-dimensional VAR models require significant resources that burst computational time when dealing with multiple epochs and subjects. This makes the Granger Causality testing process less reliable and efficient in these high-dimensional settings.

In this section, we also estimate and present the connectivities for COI in the context of data from 35 subjects pertaining to both motor execution (ME) and motor imagery (MI) tasks. The subjects performed a series of opening and closing (OC) gestures, including left-hand fist (LH), right-hand fist (RH), both fists' (BH), and both feet' (BF), for both the ME and MI tasks. The aim was to compare the brain activity associated with these tasks and gestures by identifying the patterns of connectivity and causal interactions amongst the selected channels. Each subject repeated the relevant task (i.e., task1: OC of LH/RH, task2: imagery OC of LH/RH, task3: OC of BH/BF, task4: imagery OC of BH/BF) 3 times (i.e., runs). Within these three task-oriented runs, they performed each

motor movement/imagery motion (i.e., LH, RH, BH, BF) approximately 23 times in total.

Each 64 dimensional epoch consists of about 4 seconds, that is, 640 observations. Initially, the relevant epochs were extracted from the dataset with the help of annotation information. In order to simulate a high-dimensional space for 64-dimensional EEG, we augmented the real dataset to include 170 additional signals to 64 channels by creating additional features. By increasing the dimension of each epoch, we also aimed to enrich the dataset to better capture the underlying neural dynamics. This was achieved through a series of data augmentation steps designed to capture various aspects of neural activity and connectivity. First, we generated hemispheric asymmetry channels by calculating the difference between pairs of electrodes located symmetrically across the left and right hemispheres (e.g., Fp1 - Fp2). Next, we computed anterior-posterior gradient channels by taking the difference between frontal and posterior electrode pairs (e.g., Fz - Pz). We also created lateral connectivity channels by finding differences between electrodes along the sides of the brain (e.g., FT7 - TP7). To examine central brain activities, we calculated midline activity channels by subtracting posterior midline electrodes from anterior ones (e.g., Fpz - Oz). Additionally, we computed regional average channels by averaging the signals from electrodes within specific brain regions—frontal, central, parietal, and occipital. We employed spatial derivative channels (Laplacian) by subtracting the average signal of neighboring electrodes from the signal at a central electrode (e.g., Cz minus the average of FCz, CPz, C1, and C2). This enhances the detection of localized neural activity by emphasizing differences from the surrounding area. Furthermore, we introduced product interactions between specific pairs of electrodes by multiplying their signals (e.g., F3 times P3). This captures interactions (i.e., possibly nonlinear) and joint activations between different brain regions, which might be significant for complex cognitive processes. Then, for each epoch, the high-dimensional data were reduced to COI dimensions by the proposed approach, and the estimated connectivities were recorded. From these results, the connectivities shared by at least 70% of the subjects were determined and demonstrated in Figure 5.

The GC results revealed distinct patterns of connectivity among the six channels of interest during different motor tasks, as illustrated in Figure 5. When examining left-hand motor imagery, we observed that channel C3 (left motor cortex) G-causes channel C4 (right motor cortex) and channel O1 (left occipital cortex). Channel C4 also G-causes C3, AF4 (right pre-frontal cortex), O1, and O2 (right occipital cortex). This suggests that during the imagination of left-hand movement, there is significant bilateral interaction between motor cortices and connections to occipital regions involved in visual processing.

In contrast, during left-hand motor execution, the connectivity increased. Channel C3 G-causes C4, O1, and O2, indicating that ME engages both occipital cortices more than imagery does. The involvement of both visual regions during execution may reflect the integration of sensory feedback when performing physical movements. Similarly, for right-hand tasks, during motor imagery, channel C3 G-causes C4, O1, and O2, and



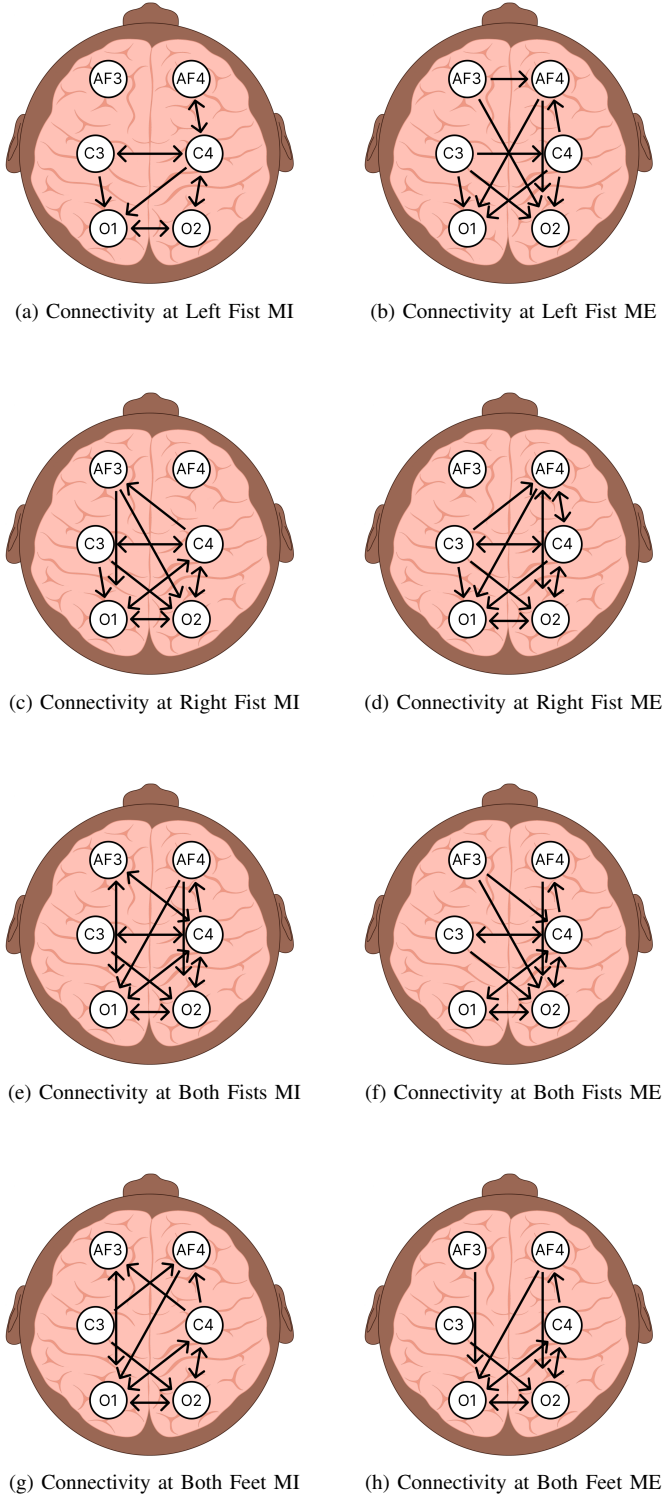


Fig. 5. Connectivity at MI vs Connectivity at ME.

channel C4 G-causes C3, AF3 (left pre-frontal cortex), O1, and O2. This pattern highlights strong bilateral connectivity and suggests that both hemispheres are actively engaged even during imagined movements.

When comparing motor imagery and execution for both fists, the connectivity patterns showed that channel C4 had extensive Granger causality to other channels during imagery, indicating the right motor cortex's central role in coordinating bilateral imagined movements. During execution, there was increased causality from AF3 and AF4 (pre-frontal cortices) to motor and occipital regions, suggesting greater involvement of executive functions and planning during actual movement. For both feet tasks, the connectivity was less pronounced, with fewer significant Granger causalities observed during both imagery and execution. This may imply that foot movements engage different neural pathways or that the linear assessment is insufficient to capture the complexity.

Overall, the contrasts between motor imagery and execution reveal that actual movement involves more extensive and complex connectivity, particularly with increased involvement of pre-frontal regions during execution.

In conclusion, the proposed approach is an easy-to-implement method for examining the connectivity between a few nodes in a high-dimensional setting. By efficiently isolating the nodes of interest and removing the confounding effects of other channels, one may focus on specific neural interactions without the computational burden of analyzing the entire high-dimensional network.

## V. DISCUSSION AND CONCLUSION

Our study aimed to enhance the accuracy of Granger causality analysis in high-dimensional time-series networks, focusing on EEG datasets. By using the sDPCA method, we effectively isolated the channels of interest from the influence of other channels in the network. Results from both simulation studies and real EEG signal analysis demonstrate the simplicity and effectiveness of our proposed method.

We found that the method maintained high accuracy with a moderate number of influencing nodes. However, its accuracy decreased as the number of influencing nodes increased or when the network approached super connectivity, like swarm-like neuronal connections. This highlights the sensitivity of Granger causality to external influences and emphasizes the need to accurately model such complexities in real-world data.

Applying the proposed approach to EEG signal networks provided empirical validation of its utility. The principal component scores derived from the spectral domain accurately captured the temporal dynamics of the high-dimensional signals. After applying sDPCA, we observed a convergence towards stationarity in the serial correlation amplitudes, bringing the data closer to the assumptions required for reliable Granger causality testing. Comparing the results before and after isolation revealed spurious causality identifications in the pre-isolation data, underlining the importance of removing extraneous influences for accurate causality assessment.

Despite these promising findings, there are some limitations to our study. The simulation framework, while comprehensive,

may not capture all nuances of real EEG data. Additionally, the test results can be significantly affected by the choice of hyperparameters, such as the number of principal components, the weights, and the number of influencing nodes. These parameters need to be carefully selected based on the specific characteristics of the datasets under study. Furthermore, our method relies on linearity-based PCA in the frequency domain, assuming that the underlying temporal dynamics can be adequately captured, which may not always hold true. Future research should consider integrating sDPCA with approaches that capture nonlinear relationships. To further improve the robustness and accuracy of causal inference in complex networks, exploring other dimensionality reduction techniques and advanced Granger causality methods would be beneficial. Moreover, the applicability of the methodology could be enhanced by including more sophisticated models of external influences and by incorporating real-time analysis capabilities.

Overall, our proposed approach offers a practical solution for isolating and analyzing causal associations in high-dimensional time series networks. Its ability to accurately identify causal connections while mitigating the effects of confounding influences makes it a valuable tool for researchers in neuroscience and other fields dealing with complex signals. The encouraging results of the study suggest that this method can improve the reliability of causality analysis, leading to more accurate and insightful investigations of the causal dynamics in high-dimensional networks.

## VI. ACKNOWLEDGMENTS

We acknowledge the assistance of Grammarly and DeepL AI tools for grammar checks and language enhancement during the preparation of this manuscript.

## REFERENCES

- [1] Markus Kalisch and Peter Bühlmann. Causal structure learning and inference: a selective review. *Quality Technology & Quantitative Management*, 11(1):3–21, 2014.
- [2] Yuxiao Wang, Chee-Ming Ting, and Hernando Ombao. Modeling effective connectivity in high-dimensional cortical source signals. *IEEE Journal of Selected Topics in Signal Processing*, 10(7):1315–1325, 2016.
- [3] Chee-Ming Ting, Abd-Krim Seghouane, and Sh-Hussain Salleh. Estimation of high-dimensional connectivity in fmri data via subspace autoregressive models. In *2016 IEEE Statistical Signal Processing Workshop (SSP)*, pages 1–5. IEEE, 2016.
- [4] Chee-Ming Ting, Hernando Ombao, S Balqis Samdin, and Sh-Hussain Salleh. Estimating dynamic connectivity states in fmri using regime-switching factor models. *IEEE transactions on medical imaging*, 37(4):1011–1023, 2017.
- [5] Yuxiao Wang, Chee-Ming Ting, Xu Gao, and Hernando Ombao. Exploratory analysis of brain signals through low dimensional embedding. In *2019 9th International IEEE/EMBS Conference on Neural Engineering (NER)*, pages 997–1002. IEEE, 2019.
- [6] Tahereh S Zarghami and Karl J Friston. Dynamic effective connectivity. *Neuroimage*, 207:116453, 2020.
- [7] Elsa Siggiridou and Dimitris Kugiumtzis. Dimension reduction of polynomial regression models for the estimation of granger causality in high-dimensional time series. *IEEE Transactions on Signal Processing*, 69:5638–5650, 2021.
- [8] Ali Shojaie and Emily B Fox. Granger causality: A review and recent advances. *Annual Review of Statistics and Its Application*, 9(1):289–319, 2022.
- [9] Y Samuel Wang and Mathias Drton. High-dimensional causal discovery under non-gaussianity. *Biometrika*, 107(1):41–59, 2020.
- [10] Sumanta Basu, Sreyoshi Das, George Michailidis, and Amiyatosh Purnanandam. A high-dimensional approach to measure connectivity in the financial sector. *The Annals of Applied Statistics*, 18(2):922–945, 2024.
- [11] David R Brillinger. The canonical analysis of stationary time series. *Multivariate analysis*, 2:331–350, 1969.
- [12] David R Brillinger. *Time series: data analysis and theory*. SIAM, 2001.
- [13] David S Stoffer. Detecting common signals in multiple time series using the spectral envelope. *Journal of the American Statistical Association*, 94(448):1341–1356, 1999.
- [14] Siegfried Hörmann, Łukasz Kidziński, and Marc Hallin. Dynamic functional principal components. *Journal of the Royal Statistical Society Series B: Statistical Methodology*, 77(2):319–348, 2015.
- [15] Hernando Ombao and Moon-ho Ringo Ho. Time-dependent frequency domain principal components analysis of multichannel non-stationary signals. *Computational statistics & data analysis*, 50(9):2339–2360, 2006.
- [16] Hernando Ombao and Marco Pinto. Spectral dependence. *Econometrics and Statistics*, 2022.
- [17] Robert H Shumway, David S Stoffer, and David S Stoffer. *Time series analysis and its applications*, volume 3. Springer, 2000.
- [18] Gerwin Schalk, Dennis J McFarland, Thilo Hinterberger, Niels Birbaumer, and Jonathan R Wolpaw. Bci2000: a general-purpose brain-computer interface (bci) system. *IEEE Transactions on biomedical engineering*, 51(6):1034–1043, 2004.
- [19] Alexandre Gramfort, Martin Luessi, Eric Larson, Denis A. Engemann, Daniel Strohmeier, Christian Brodbeck, Roman Goj, Mainak Jas, Teon Brooks, Lauri Parkkonen, and Matti S. Hämäläinen. MEG and EEG data analysis with MNE-Python. *Frontiers in Neuroscience*, 7(267):1–13, 2013.
- [20] Eric Larson, Alexandre Gramfort, Denis A Engemann, and et collab. *MNE-Python*, <https://doi.org/10.5281/zenodo.10519948>. Zenodo, January 2024.

## APPENDIX

TABLE III

ACCURACY RESULTS FOR VARYING NUMBERS OF INFLUENCING NODES WITH LINEAR INFLUENCE AND WEIGHTS ON THE COI IN A HIGH-DIMENSIONAL NETWORK UNDER A NON-NORMAL ERROR DISTRIBUTION,  $\epsilon \sim \text{non-Norm}(\mu = -1, \sigma = 1, \gamma = 1.5, \kappa = 3.5)$ . THE COI CONSISTS OF THE FIRST 40 NODES OUT OF A TOTAL OF 512 NODES. THE NUMBERS 30 TO 120 REPRESENT THE NOF INFLUENCING THE COI, AND THE VALUES 0.1 TO 0.7 REPRESENT THE WEIGHTS OF THIS INFLUENCE.

Influencing Nodes = 30				
Ndpc	wt = 0.1	wt = 0.3	wt = 0.5	wt = 0.7
3	0.89	0.80	0.73	0.71
6	0.87	0.76	0.73	0.69
12	0.87	0.79	0.76	0.65
24	0.87	0.78	0.70	0.73
Influencing Nodes = 60				
Ndpc	wt = 0.1	wt = 0.3	wt = 0.5	wt = 0.7
3	0.84	0.74	0.64	0.60
6	0.86	0.77	0.66	0.62
12	0.84	0.69	0.63	0.62
24	0.81	0.76	0.60	0.62
Influencing Nodes = 90				
Ndpc	wt = 0.1	wt = 0.3	wt = 0.5	wt = 0.7
3	0.85	0.74	0.60	0.63
6	0.82	0.70	0.62	0.62
12	0.86	0.69	0.63	0.63
24	0.75	0.70	0.61	0.63
Influencing Nodes = 120				
Ndpc	wt = 0.1	wt = 0.3	wt = 0.5	wt = 0.7
3	0.82	0.61	0.62	0.64
6	0.78	0.62	0.62	0.63
12	0.88	0.67	0.63	0.64
24	0.83	0.66	0.62	0.64

TABLE IV

ACCURACY RESULTS FOR VARYING NUMBERS OF INFLUENCING NODES WITH LINEAR INFLUENCE AND WEIGHTS ON THE COI IN A HIGH-DIMENSIONAL NETWORK UNDER A HEAVY-TAILED ERROR MECHANISM WITH  $\epsilon \sim t_{(d.o.f=8)}$ . THE COI CONSISTS OF THE FIRST 40 NODES OUT OF A TOTAL OF 512 NODES. THE 30, 60, 90, AND 120 REPRESENT THE NOF NODES INFLUENCING THE COI, AND THE VALUES 0.1, 0.3, 0.5, AND 0.7 REPRESENT THE WEIGHTS OF THIS INFLUENCE.

Influencing Nodes = 30				
Ndpc	wt = 0.1	wt = 0.3	wt = 0.5	wt = 0.7
3	0.94	0.80	0.75	0.71
6	0.93	0.79	0.74	0.72
12	0.93	0.83	0.73	0.64
24	0.86	0.78	0.74	0.69
Influencing Nodes = 60				
Ndpc	wt = 0.1	wt = 0.3	wt = 0.5	wt = 0.7
3	0.92	0.73	0.71	0.63
6	0.88	0.77	0.63	0.62
12	0.88	0.73	0.66	0.61
24	0.82	0.77	0.63	0.62
Influencing Nodes = 90				
Ndpc	wt = 0.1	wt = 0.3	wt = 0.5	wt = 0.7
3	0.81	0.74	0.60	0.62
6	0.87	0.71	0.63	0.63
12	0.83	0.76	0.62	0.62
24	0.85	0.78	0.62	0.63
Influencing Nodes = 120				
Ndpc	wt = 0.1	wt = 0.3	wt = 0.5	wt = 0.7
3	0.78	0.65	0.63	0.64
6	0.82	0.70	0.63	0.63
12	0.85	0.69	0.62	0.64
24	0.79	0.72	0.63	0.63

TABLE V

ACCURACY RESULTS FOR VARYING NUMBERS OF INFLUENCING NODES WITH LINEAR INFLUENCE AND WEIGHTS ON THE COI IN A HIGH-DIMENSIONAL NETWORK UNDER A GAUSSIAN ERROR MECHANISM. THE COI CONSISTS OF THE FIRST 40 NODES OUT OF A TOTAL OF 512 NODES. THE NUMBERS 30, 60, 90, AND 120 REPRESENT THE NUMBER OF NODES INFLUENCING THE COI, AND THE VALUES 0.1, 0.3, 0.5, AND 0.7 REPRESENT THE WEIGHTS OF THIS INFLUENCE.

Influencing Nodes = 30				
Ndpc	wt = 0.1	wt = 0.3	wt = 0.5	wt = 0.7
3	0.92	0.77	0.74	0.66
6	0.93	0.78	0.71	0.70
12	0.89	0.80	0.79	0.65
24	0.85	0.83	0.71	0.67
Influencing Nodes = 60				
Ndpc	wt = 0.1	wt = 0.3	wt = 0.5	wt = 0.7
3	0.93	0.73	0.71	0.61
6	0.87	0.71	0.61	0.62
12	0.82	0.72	0.65	0.64
24	0.82	0.73	0.63	0.62
Influencing Nodes = 90				
Ndpc	wt = 0.1	wt = 0.3	wt = 0.5	wt = 0.7
3	0.86	0.69	0.63	0.62
6	0.80	0.72	0.62	0.62
12	0.85	0.73	0.63	0.63
24	0.84	0.68	0.62	0.63
Influencing Nodes = 120				
Ndpc	wt = 0.1	wt = 0.3	wt = 0.5	wt = 0.7
3	0.88	0.66	0.61	0.63
6	0.86	0.64	0.63	0.64
12	0.80	0.64	0.62	0.63
24	0.81	0.68	0.61	0.64

TABLE VI

ACCURACY RESULTS FOR VARYING NUMBERS OF INFLUENCING NODES WITH NONLINEAR INFLUENCE AND WEIGHTS ON THE COI IN A HIGH-DIMENSIONAL NETWORK UNDER A HEAVY-TAILED ERROR MECHANISM WITH  $\epsilon \sim t_{(d.o.f=8)}$ . THE COI CONSISTS OF THE FIRST 40 NODES OUT OF A TOTAL OF 512 NODES. THE 30, 60, 90, AND 120 REPRESENT THE NOF NODES INFLUENCING THE COI, AND THE VALUES 0.1, 0.3, 0.5, AND 0.7 REPRESENT THE WEIGHTS OF THIS INFLUENCE.

Influencing Nodes = 30				
Ndpc	wt = 0.1	wt = 0.3	wt = 0.5	wt = 0.7
3	0.97	0.87	0.68	0.64
6	0.95	0.82	0.69	0.63
12	0.93	0.80	0.64	0.63
24	0.91	0.86	0.67	0.64
Influencing Nodes = 60				
Ndpc	wt = 0.1	wt = 0.3	wt = 0.5	wt = 0.7
3	0.94	0.80	0.63	0.65
6	0.95	0.80	0.63	0.64
12	0.97	0.79	0.63	0.65
24	0.91	0.79	0.62	0.65
Influencing Nodes = 90				
Ndpc	wt = 0.1	wt = 0.3	wt = 0.5	wt = 0.7
3	0.90	0.74	0.63	0.64
6	0.95	0.76	0.63	0.65
12	0.92	0.75	0.64	0.65
24	0.93	0.76	0.65	0.64
Influencing Nodes = 120				
Ndpc	wt = 0.1	wt = 0.3	wt = 0.5	wt = 0.7
3	0.93	0.72	0.64	0.64
6	0.91	0.66	0.65	0.64
12	0.89	0.65	0.64	0.65
24	0.88	0.63	0.66	0.64

TABLE VII

ACCURACY RESULTS FOR VARYING NUMBERS OF INFLUENCING NODES WITH NONLINEAR INFLUENCE AND WEIGHTS ON THE COI IN A HIGH-DIMENSIONAL NETWORK UNDER A GAUSSIAN ERROR MECHANISM. THE COI CONSISTS OF THE FIRST 40 NODES OUT OF A TOTAL OF 512 NODES. THE NUMBERS 30, 60, 90, AND 120 REPRESENT THE NUMBER OF NODES INFLUENCING THE COI, AND THE VALUES 0.1, 0.3, 0.5, AND 0.7 REPRESENT THE WEIGHTS OF THIS INFLUENCE.

Influencing Nodes = 30				
Ndpc	wt = 0.1	wt = 0.3	wt = 0.5	wt = 0.7
3	0.92	0.78	0.71	0.64
6	0.95	0.80	0.63	0.64
12	0.94	0.80	0.66	0.64
24	0.93	0.80	0.68	0.63
Influencing Nodes = 60				
Ndpc	wt = 0.1	wt = 0.3	wt = 0.5	wt = 0.7
3	0.94	0.78	0.63	0.65
6	0.97	0.74	0.63	0.65
12	0.93	0.81	0.62	0.64
24	0.92	0.75	0.63	0.65
Influencing Nodes = 90				
Ndpc	wt = 0.1	wt = 0.3	wt = 0.5	wt = 0.7
3	0.97	0.69	0.64	0.64
6	0.91	0.67	0.65	0.64
12	0.90	0.73	0.64	0.64
24	0.91	0.68	0.65	0.65
Influencing Nodes = 120				
Ndpc	wt = 0.1	wt = 0.3	wt = 0.5	wt = 0.7
3	0.92	0.64	0.64	0.64
6	0.89	0.59	0.65	0.64
12	0.93	0.69	0.65	0.64
24	0.86	0.63	0.64	0.65